ELSEVIER

Polymer 43 (2002) 4421–4436

polymer

www.elsevier.com/locate/polymer

Controlled local organization of lyotropic liquid crystalline polymer thin films with electric fields

David C. Martin*,[1]

Department of Materials Science and Engineering, Biomedical Engineering and the Macromolecular Science and Engineering Centre, The University of Michigan, 2022 H.H. Dow Building, Ann Arbor, MI 48109-2136, USA

Received 27 November 2001; received in revised form 1 April 2002; accepted 3 April 2002

Abstract

The ability of electric fields to induce the controlled alignment of lyotropic liquid crystalline polymer thin films on microfabricated substrates is demonstrated. These devices allow for variations in electric field geometry on the polymer alignment to be examined systematically. The polymers studied included poly(hexyl isocyanate) (PHIC) and poly(benzyl L-glutamate). The polymers were oriented by the electric field while in solution and solidified into a stable, oriented structure by solvent evaporation. Optical microscopy and transmission electron microscopy experiments make it possible to directly image the disclinations that mediate molecular alignment. The defect type and density in the solidified films are a function of the electric field geometry.

Keywords: Liquid crystalline polymer; Electric field geometry; Poly(hexyl isocyanate)

1. Overview

The ability to direct the local organization of polymer materials through the rational design of chemical structure and processing methods is of continuing scientific and technological interest [1]. One means to guide the development of desirable microstructures is by using an externally applied field. These gradients in thermodynamic potential may be either chemical, mechanical, magnetic, or electrical in origin. Electric fields are of particular utility because of the degree of precision that can be exerted over the magnitude and dynamics of the field and the ability to create micromachined electrodes of well-defined size and shape.

Controlling the orientation of organic molecules with electric fields plays an important role in commercially important devices, such as liquid crystalline displays. The use of electric fields to change flow behavior (electrorheology) is also of considerable current interest [2]. Electric fields have the potential to rapidly create materials in which all of the molecular dipoles are oriented in the same direction, which is important for non-linear optics and electrostriction [3]. The ability to freeze in dipole orientation in polymers has lead to the production of 'electrets', which are the electrostatic equivalents of magnets [4]. Polymer electrets constructed from materials such as poly(vinylidene fluoride) (PVF_2) are used commercially in devices as microphones and earphones.

Because liquid crystalline polymers (LCPs) can be readily aligned in shear fields and the oriented microstructure trapped in place during coagulation from solution, they have been technologically useful for creating high strength fibers for lightweight structural applications. LCPs can also exhibit dramatic alignment effects in magnetic and electric fields. Hudson and Thomas [5] investigated the stability of disclination interactions of thermotropic LCP thin films in magnetic fields by transmission electron microscopy (TEM). The length scale of the observed distortions was related to the ratio between the energy for distortions to the driving force for alignment in the field. Körner et al. [6] and Shiota and Ober [7] created aligned samples of liquid crystalline thermosets by curing in an alternating current (AC) electric field. The structure evolution during curing was monitored by in situ X-ray diffraction. However, in these experiments the electric field was uniform, and the limited spatial resolution made it problematic to discern the local mechanisms of alignment.

Morkved et al. [8] have described a novel approach for examining ordered polymer thin films using self-supported

* Tel.: +1-734-936-3161; fax: +1-734-763-4788.
E-mail address: milty@umich.edu (D.C. Martin).
[1] www-personal.engin.umich.edu/~milty; msewww.engin.umich.edu/people/milty

0032-3861/02/$ - see front matter
PII: S0032-3861(02)00256-2

amorphous silicon nitride membranes grown on single crystal silicon substrates. PMMA–PS diblock copolymers were oriented in the plane by an electric field applied between lithographically defined metallic contacts. A significant advantage of this approach was the possibility to evaluate the local structure of the oriented film by TEM. An additional feature was that corroborative information could be obtained from other techniques such as atomic force microscopy [9]. The images provided information about the defect-mediated mechanisms of alignment in these microphase-separated block copolymers, including the identification of individual edge dislocations which accommodated the deformation in regions where the electric field was not uniform.

Here, experimental results from devices designed to corroborate and extend the seminal work of Morkved et al. [8,9] is described. These new designs provide for systematic variations in the geometry of the electric field by changing the configuration of the metallic electrodes (Fig. 1). The field of view was also enlarged considerably (to 1 mm × 1 mm) in order to better facilitate complimentary studies by optical microscopy (OM).

The utility of these substrates was confirmed by examining the microstructures of the lyotropic LCPs poly(hexyl isocyanate) (PHIC) and poly(benzyl L-glutamate) (PBLG). Other polymer materials of current interest were investigated. The results revealed that electric fields can rapidly induce a high degree of controlled, local structural organization in LCPs that have a strong dipole along the molecular chain. These results provide insight about the defect structures, which develop in LCPs during solution processing. It is anticipated that further work of this sort will continue to provide quantitative information about the relationship between the microstructure and macroscopic properties of ordered polymer thin films. Some possible future variations on this approach to manipulate the local microstructural ordering of polymers at the nanometer length scale are also discussed.

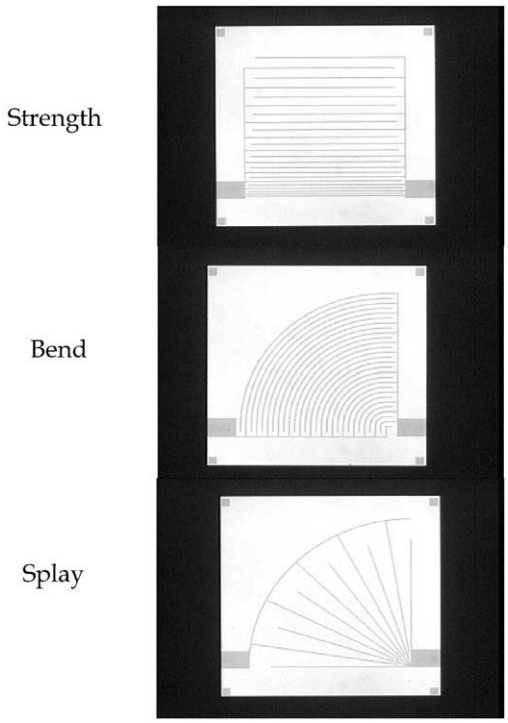

Fig. 1. Optical micrographs of the three device designs: (a) strength; (b) bend; and (c) splay.

2. Background

The influence of an electric field on the free energy of microphase-separated block copolymers has been discussed by Amundson et al. [10] on the basis of the differences in local dielectric constant between the domains of the phase-separated block copolymer. For cylindrical microphases in a uniform field, the energy is minimized when the axis of the cylinders lies parallel to the axis of the external field. For non-uniform fields, the configuration of the microstructure which minimizes the energy is expected to be more complex.

We focused our attention here on the orientation of lyotropic LCPs which have a strong dipole moment in the backbone of the molecule. For these polymers, the influence of the external electric field was expected to be even more profound. Since the materials of present interest were processed from solution, the results obtained correspond to the organization which is induced in the polymer thin film during the loss of solvent. These solidification processes may include phase separation, crystallization, and vitrification.

The energy for the distortions of a nematic liquid crystalline material has been discussed by Frank [11]. In the absence of a field, the energy for the distortions of a nematic liquid crystal is given by

$$F_n = \frac{1}{2}\int \mathrm{d}^3x\left\{K_1(\nabla\cdot n)^2 + K_2[n\cdot(\nabla\times n)]^2 + K_3[n\times(\nabla\times n)]^2\right\}$$

where n is a vector locally parallel to the molecular director field and K_1, K_2 and K_3 are elastic coefficients for splay, twist and bend, respectively. When there is an applied electric field, there is an additional term in the free energy [10,12]

$$F_\mathrm{e} = -\frac{1}{8\pi}\int \varepsilon(r)|E(r)|^2\,\mathrm{d}^3r$$

where $\varepsilon(r)$ is the local dielectric anisotropy. This term may arise from an inherent dipole moment in the molecular or helical structure, or may also develop due to local variations in the isotropic dielectric properties of the components of an anisotropic microphase-separated structure. In block-copolymers both effects will be important, and it is likely that the competition between them may be used to further tailor the response to an external electric field.

For systems which are oriented in an external aligning field, it is possible to define a characteristic length which relates the elastic energy of the distortions due to variations in the director field with the energy of alignment. The resulting length scale is the electric coherence length ξ_e

$$\xi_e = \sqrt{\frac{4\pi K}{\varepsilon_a E^2}}$$

where K is an average elastic constant for splay, twist, and bend; ε_a, the dielectric anisotropy; E is the applied electric field.

At sample dimensions above this characteristic length, the forces on the structure are dominated by the aligning field, whereas below this dimension the forces are predominantly due to the mechanical distortions of the director pattern [10]. Possible aligning fields include electric fields, magnetic fields, and deformation fields due to externally applied shear or extensional flow gradients [5]. These introduce corresponding characteristic lengths ξ_m, $\xi_{\dot{\varepsilon}}$, and ξ_γ :

$$\xi_m = \sqrt{\frac{K}{\chi_a H^2}}$$

$$\xi_{\dot{\varepsilon}} = \sqrt{\frac{K}{2|\alpha_3 + \alpha_2|\dot{\varepsilon}}}$$

$$\xi_\gamma = \sqrt{\frac{K}{4|\alpha_3\alpha_2|^{1/2}\dot{\gamma}}}$$

The distortions observed in the director field of a LCP after crystallization were similar to those seen in magnetic and electric fields, and it is therefore proposed that a similar parameter should be useful to characterize the length scale of this process as well. We anticipate that such a length scale $\xi_{\Delta H_c}$ will be defined by the ratio of the elastic distortion (determined by K) and the driving force for crystallization, determined by the energy associated with crystallization, as estimated by the heat of fusion ΔH_c:

$$\xi_{\Delta H_c} = \sqrt{\frac{K}{\Delta H_c}}$$

3. Device design and fabrication

The devices used by Morkved et al. [8,9] consisted of a two-electrode geometry, with a 60 μm window area. Devices were constructed having three unique variations in the nature of the electric field (Fig. 1). The electrodes themselves were constructed from 5 μm wide gold lines with a nominal thickness 25 nm. The amorphous silicon nitride membrane was 75 nm thick. The devices were constructed at the Cornell National Nanofabrication Facility

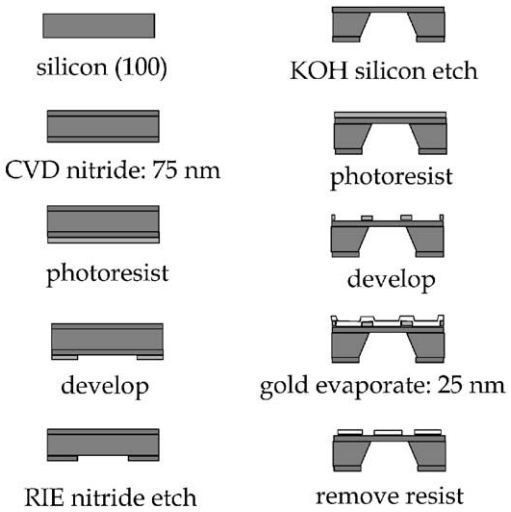

Fig. 2. Process steps used at the Cornell National Nanofabrication Facility to create the devices used in this study.

(NNF) as described by Morkved et al. [9] as shown schematically in Fig. 2. The process involves depositing a nitride layer by CVD, followed by deposition of photoresist and a deep etch to create a self-supported thin membrane. During the manufacturing of the devices, it was attempted to shorten the number of necessary processing steps by first depositing the gold electrodes before the deep silicon etch required to open the windows to the silicon nitride. Unfortunately, the gold lines were damaged by deep KOH etching step, so this route was not successful. Four 80 mm wafers were eventually produced, with each wafer containing roughly equal amounts of the three different device designs. There were approximately 400 devices on each wafer, which were then broken out for testing. The larger silicon nitride membranes proved to be fairly sensitive to large mechanical shocks, so that particular care was required in breaking the wafers along the scribed lines. Good results were obtained by holding the remainder of the wafer securely on a glass plate during cleavage.

The designs of the electrodes themselves are shown in Fig. 1. There were three different geometries created which were called (1) strength, (2) bend, and (3) splay. All three of the devices were constructed with a 1 mm × 1 mm (1000 μm × 1000 μm) silicon nitride window in the center of a 3 mm × 3 mm square device. The size of the substrates was such that they could be directly mounted in a conventional TEM sample holder. Electrical contact was facilitated by 1 mm × 3 mm gold electrodes deposited on either side of the device. Contact between these larger mounting pads and the patterned electrodes was achieved with a 100 μm wide line, as shown in the schematic diagram. Four 25 μm gold squares were placed at the corners of the central silicon nitride window to help facilitate alignment during wafer processing and the calibration of TEM images and electron diffraction patterns.

The specific characteristics of the three device geometries created were (Fig. 1) as follows:

1. *Strength*. Five micrometers wide electrodes at a constant gap spacing, with a minimum distance of 6 μm, increasing in steps of 2 μm to a maximum gap distance of 48 μm. This design results in an electric field in which there are systematic variations in field strength.
2. *Bend*. Five micrometer wide electrodes at a constant gap spacing of 20 μm, but with increasing radii of curvature from a minimum of 0–20 μm (min–max) up to a maximum of 675–695 μm in an incremental steps of 25 μm. This design results in an electric field in which there are variations in the local divergence (i.e. the field lines splay).
3. *Splay*. Five micrometer wide electrodes with a constant angle of separation between the electrodes of 9°, resulting in 10 equivalent sectors over 90°. This design leads to an electric field in which there are variations in the curvature (i.e. the field lines bend).

The motivation behind these new designs was to provide substrates in which the influence of these systematic variations in the electric field geometry on microstructural organization could be examined on the same polymer film processed under a given set experimental conditions. It was also desired to monitor the evolution of the structure using polarized light OM, which was facilitated by the enhanced field of view. The fact that the spacings between the elemental composition of the gold lines were known also made the substrates convenient for the real and reciprocal space calibration of TEM images and selected area electron diffraction patterns.

The materials chosen as the focus of this study were PHIC and PBLG. Both of these are lyotropic LCPs which can be conveniently processed from non-polar solvents, and have been studied in considerable detail in previous investigations. The chemical repeat structures of these two polymers are shown in Fig. 3.

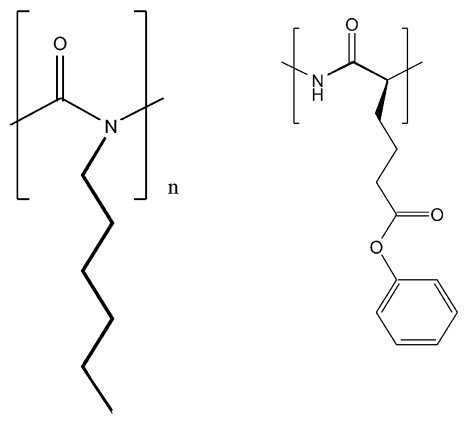

Fig. 3. Chemical structures of (a) PHIC and (b) PBLG.

3.1. PHIC

The structure and properties of poly(alkyl isocyanates) were reviewed by Bur and Fetters [13]. Aharoni [14] has recently published a monograph on the synthesis, structure, and properties of *n*-nylons, which included a chapter on 1-nylons, the polyisocyanates. Poly(alkyl isocyanates) contain alternating carbonyl and amino-alkyl groups along the backbone of the molecule. In solution, the polymers adopt a helical conformation, which appears to be most stable as a roughly eightfold helix. The 8_3 helical structure was argued to be consistent with X-ray diffraction data on PBIC by Shmueli et al. [15] and has been supported by energetic calculations by Troxell and Scheraga [16,17].

Poly(alkyl isocyanates) exhibit 'worm-like' behavior in solution, with values of the Mark–Houwink exponent a for PHIC ranging from 0.92 to 1.4, depending on the solvent [14]. The estimated persistence length of the chain ranges from 35 to 42 nm, and the characteristic ratio has been estimated to be in the order of 400. The poly(isocyanates) have been shown to exhibit both lyotropic and thermotropic liquid crystallinity for side chain alkyl group lengths from $n = 4$ to 11 [14]. The susceptibility of the rigid, helical poly(alkyl isocyanates) to electric field orientation is shown by measurements of the Kerr constant $K = (\Delta n/cE^2)$, with Δn the difference in refractive index parallel and perpendicular to the applied field E, with c the concentration. The value of K is 5.5×10^{-7} for the helical poly(*n*-chlorohexyl isocyanate), while it is only 2.25×10^{-12} for non-helical poly(tolylisocyanate), which is more typical of a flexible-coil polymer [18].

The worm-like nature of the poly(alkyl isocyanate) chains is also evident from estimates of the dipole moment per repeat unit as a function of molecular weight, as obtained from measurements of the static dielectric constant [19]. At low molecular weights ($n < 10^3$), the dipole moment per repeat unit (μ/n) approached an asymptotic limit of 1.13 D for poly(butyl isocyanate), which was directed along the long axis of the molecule. This value decreased with increasing molecular weight in a manner consistent with the Kratky–Porod model for a worm-like chain. For values of $n > 10^4$, the conformation was essentially random-coil, with μ/n asymptotically approaching zero with increasing chain length.

The precise crystalline structure of PHIC has not yet been determined unambiguously. Chen et al. [20] have presented the most detailed analysis to date on PHIC containing rod-coil block copolymers, and asserted that their electron diffraction results were consistent with an eightfold helix arranged on a two-chain, pseudo-hexagonal lattice ($a = b = 1.51$ nm, $c = 1.56$ nm) (Fig. 4). This 8_3 helical conformation is similar to that proposed by Shmueli et al. for crystalline PBIC. However, the conformation of the alkyl side groups in the unit cell has not been determined, and a detailed match of the experimental results to a crystal model for crystalline PHIC has not been obtained. It is not

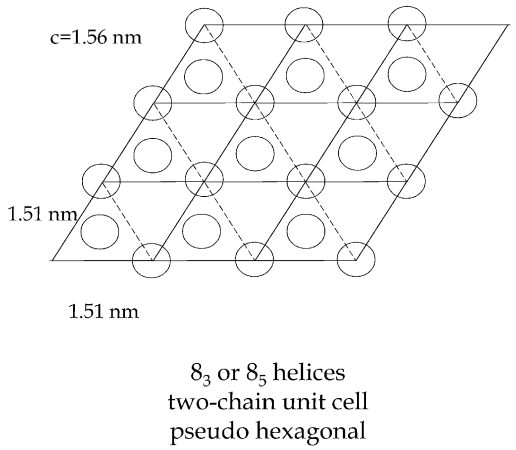

Fig. 4. Schematic unit cell for crystalline PHIC based on the analysis by Chen et al. [20,41]. There are two chains per unit cell in an 8_3 helix. The lattice parameters are nominally hexagonal with $a = b = 1.51$ nm and $c = 1.56$ nm.

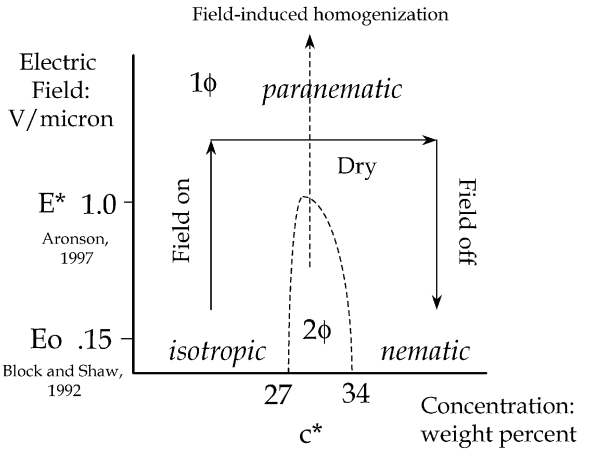

Fig. 5. Schematic phase diagram of PHIC based on the theory of Khoklov and Semenov [24] and using information available from the literature including the studies of field orientation by Block and Shaw [35], and the critical points as estimated by Aronson in 1997.

yet clear, for example, what distortions to the supposedly eightfold helical symmetry of the PHIC molecule are induced by the packing constraints provided by a locally three and sixfold hexagonal lattice. Although Chen et al. did not specifically discuss the precise placement of the molecule and the alkyl side groups in the unit cell, a schematic of one possible arrangement using their proposed unit cell parameters is shown in the diagram (Fig. 4).

In solution, PHIC is thought to adopt a stable helical conformation, and the possibility of helical reversals has been discussed. Green et al. [21] have studied the transformation of the helical hand from left to right by adding chiral substituents. Placing just a few chiral units on the chains results in dramatic cooperative behavior in which the entire molecule chooses to adopt a single helical hand. What appears to have been less completely studied, however, is the possibility of local changes in clinicity which may also occur along the backbone of the molecule. This leads to the potential for local reversals in the orientation of the dipoles in the helix with respect to the chain backbone. These variations in clinicity can in principle occur independently of the handedness of the helix.

The theories of liquid crystalline ordering developed by Onsager [22] and Flory [23] predict a two-phase 'chimney' region between a dilute isotropic phase and a more concentrated nematic phase. Khoklov and Semenov [24] extended the Onsager analysis to include the influence of an external field, and predicted that the two-phase region would be suppressed to a specific region of the phase diagram in the field–concentration plane, as shown in Fig. 5. This means it should be possible to process a LCP solution from an isotropic melt to a nematic liquid without ever passing through a first-order phase transition. The necessary pathway is indicated on the schematic phase diagram (Fig. 5). The dilute solution is first oriented by the field, then concentrated by evaporation. In this step, the microstructure is frozen in place by crystallization or vitrification of the nematic liquid crystal due to the loss of additional solvent. The microstructure would then be frozen in place and remain stable after the field is removed.

To use this concept to guide our experimental design, it is useful to have information about the characteristic concentrations and fields corresponding to our materials. Filisko et al. [25] have recently been investigating the use of PHIC as an electrorheological fluid. These experiments have included studies of the orientation and flow behavior of PHIC as a function of applied field and concentration. From these results, estimates have been obtained of the concentrations for the onset of the bi-phasic region at zero field (27 wt%), the onset of the completely nematic region (34 wt%), and the critical point ($E = 1$ V/μm, $c = 27$ wt%) [26].

To examine the dynamics of solvent evaporation and subsequent changes in structure during drying, a 'diffusion-couple' geometry was used in which the solution was placed under a cover slip and allowed to slowly evaporate from the edges. After a period of time a stable microstructure developed in which the interior of the sample remained isotropic, followed by a band of the nematic liquid crystal showing evidence for a typical Schlieren texture including both positive and negative disclination defects, and finally a crystalline layer nearest the external surface (Fig. 6). The interface between the isotropic region and the nematic was rough on a several micrometer length scale, although it was locally smooth. On the other hand, the interface between the nematic and the crystalline domains was smooth on larger length scales, but appeared locally rough. The width of the characteristic bands of texture grew with time, and measurements of these dimensions provided information about the dynamics of solvent transport and evaporation from the edge of the cover slide.

The differences in mechanical response of the various phases was readily evident by moving the cover slip slightly during the experiment. The nematic domains would flow

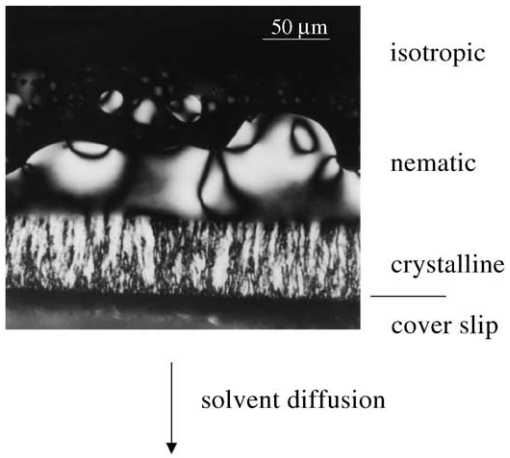

Fig. 6. Transmitted light micrograph using cross-polars of a PHIC diffusion couple. The solvent is evaporating from the interior of the sample (top) to the edge of the cover slip (bottom). The domains of crystalline PHIC, nematic PHIC, and isotropic PHIC can be readily identified from their characteristic optical textures.

readily during this process, and the disclinations were seen to move around as well. However, the crystalline zones appeared to be essentially immobile, although some evidence for kinking of the oriented, solidified polymer was observed after deformation. The crystalline layers showed a high degree of orientation parallel to the edge of the cover slip, which was apparently induced by the anisotropic geometry of solvent loss. The orientation of the molecules in the crystalline layer was confirmed to be parallel to edge the cover slip by electron diffraction. This information made it possible to map out the local orientation of the molecules in both the crystalline domains and the neighboring liquid crystalline zone by examining the sample in crossed-polarized light and monitoring the behavior of the dark extinction brushes as a function of the orientation of the sample stage [27].

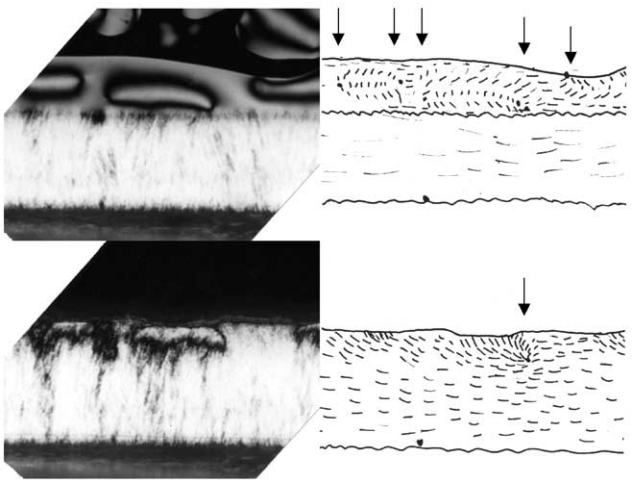

Fig. 7. Optical micrograph of a PHIC sample before (top left) and after (bottom left) the crystallization of the nematic domain. By examining the orientation of the dark brushes observed in cross-polarized light as a function of the angle of the microscope stage, it is possible to map out the local orientation of the molecular director, as shown schematically in the figures on the right.

Fig. 7 shows the change in structure near a +1/2 disclination which was unable to escape from a propagating crystallization front. The image on the left shows an optical micrograph of PHIC including the already crystallized layer on the bottom of the figure, the nematic domain with several disclination defects, and the isotropic solution at top. The orientation of the PHIC molecules was determined by rotating the sample stage under crossed-polarizers, and is sketched in Fig. 7 on the top right. The figure on the bottom left was obtained after crystallization was completed. The +1/2 disclination which was located near the growing crystal front was not able to escape or annihilate before crystallization, and therefore induced a residual distortion in the crystalline material.

Fig. 8 shows the data obtained for the orientation of the director field near the disclination. The orientation of the molecular director is plotted as a function of the azimuthal angle around the core of the defect. The estimated distance from the core for these measurements was 5 μm. The limited resolution of the optical microscope did not make it possible to look for variations as a function of distance from the defect, as was done by Hudson et al. [28]. However, this experiment confirms that the crystallization process causes a significant distortion of the director pattern. The change shows a localization of the deformation in a manner reminiscent of that induced by an applied electric or magnetic field. It therefore seems appropriate to consider the process of the crystallization of this

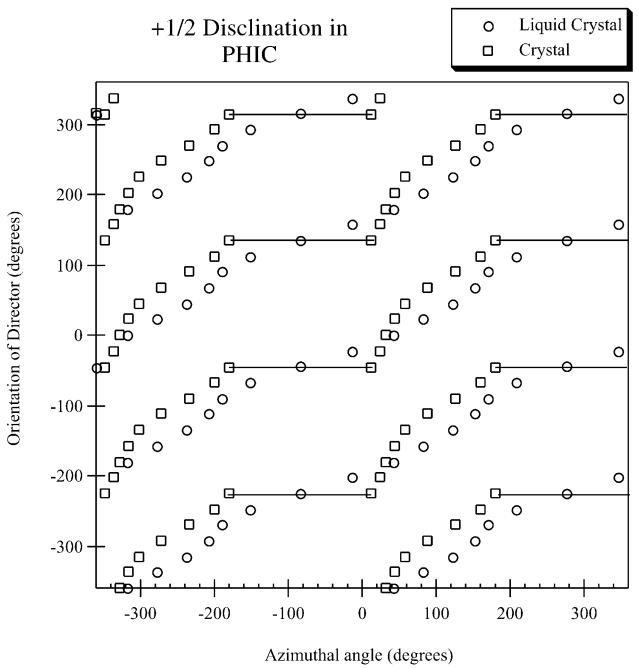

Fig. 8. Plot of the orientation of the PHIC molecules as a function of azimuthal angle near the core of crystallized disclination. The distortions induced in the orientation of the director are similar to that produced by an external field.

polymeric liquid crystal as somewhat similar to that of an applied field.

3.2. PBLG

Poly(γ-benzyl L-glutamate) is a model synthetic polypeptide which adopts a rigid 18_5 alpha-helical conformation in solution. Measurements of the dipole moment of PBLG as a function of molecular weight give an estimated value of approximately 3 D per repeat unit for degrees of polymerization below $n < 10^3$ [29]. PBLG has been investigated by a number of different groups, and in particular has been used as a model system to study structural evolution in LCPs during solution processing [30,31]. Evidence for several crystalline unit cells have been observed including form B, which is monoclinic with two chains per unit cell in opposite orientations, forms D and E, with 7 and 19 chains per cell, respectively, and form C, which is nearly hexagonal and has random orientations of the chains [32]. PBLG is also known to form crystal solvate phases with solvents, including the A and B complexes with benzyl alcohol [33,34].

4. Electric field alignment

Block and Shaw [35] investigated the application of an electric field to both PHIC and PBLG. The PHIC was cast from toluene, and the PBLG from chloroform or dioxane. The films were obtained by evaporation between stainless steel electrodes mounted on a glass slide. The maximum voltage used was 3 kV direct current (DC), with a 3 mm electrode separation. The extent of orientation was determined by measuring the efficiency of second-order harmonic generation. For PHIC, it was found that a field greater than 0.15 V/μm was necessary to induce significant orientation. For PBLG, local variations in the orientation were found, and were associated with a complex film morphology, including the possibility of a cholesteric phase. However, the local structure of the oriented films was not examined in detail.

4.1. Instruments and procedures

External contact to the electrodes of the device was provided by attaching thin wires held in place with adhesive tape. A jig was also constructed for the optical microscope by Alexander DuChesne which allowed for rapid attachment of the devices to the electric field. This also avoided the possibility of solvent swelling the adhesive tape, which was occasionally found to lead to loss of electrical contact over a period of time. This jig was machined from glass and had spring-loaded clips with attached metal wires. The area under the device was machined away to allow for light to pass cleanly through the sample without interference with the glass substrate.

The DC potential was provided by a Physik Instrument P-263 High Voltage Power Supply capable of a maximum of 1000 V. An AC potential was obtained using a Kontron Messtechnik 20 MHz pulse/function generator connected to an amplifier. The usual frequency used was 50 Hz.

OM was performed on a Zeiss Axiophot in both transmitted and reflected polarized light. Images were recorded on 35 mm film and with a video camera. The experimental question of whether the substrates were properly connected to the electric field could be readily determined before any polymer solution was deposited by monitoring the devices in reflected light. At low fields the silicon nitride substrate showed fluctuations in contrast due to small variations in the local orientation of the film surface. However, when an AC potential greater than ~96 V was applied, the substrate responded by flattening, leading to the elimination of the wrinkles in the film. This behavior was rapid and reproducible, and was observed at a variety of different applied frequencies. The sensitivity of the silicon nitride membrane to respond to rapid changes in air currents in the room (such as from loud noise) was also obvious in this arrangement.

After the substrate was connected to the field, the voltage of the power supply was increased. It was found that there was a plateau region in the observed DC potential which could be developed across the sample. During testing the sample was usually held at a potential just below the onset of this plateau. The value of the voltage used was typically 30 V. At the highest voltages, there was evidence for dielectric breakdown, detected as a buzzing noise from the sample which was heard to initiate around 300 V.

The polymer film was placed on the device by direct deposition of a single droplet from a glass pipette. This was usually done while the substrate mounted on the stage of the optical microscope so that the progress of solvent evaporation could be monitored directly. The more volatile chloroform (solvent for PBLG) was evaporated in a short time, with the total time for the droplet to dry estimated to be less than 30 s. For xylene (solvent for PHIC), the evaporation was significantly slower, with the characteristic time estimated to be in the order of 5 min. Fig. 9 shows a time series for the solvent evaporation process as imaged in the optical microscope. The onset of orientation and subsequent freezing-in of the polymer microstructure was evident only in the last stages of the drying process.

TEM was performed on a 120 kV Philips CM 12 using a LaB_6 filament and a 120 kV Zeiss 912 equipped with an Omega energy filter. This latter instrument makes it possible to obtain significantly improved electron diffraction patterns of polymers by eliminating the contribution from inelastically scattered electrons [36]. This was particularly useful for investigating spacings at low angles which are otherwise very difficult to resolve due to the intense inelastic peak.

4.2. Materials

The PHIC was provided in powder form from Prof. Frank E. Filisko at the University of Michigan. A stock solution of nominal concentration 1 wt% was prepared using *m*-xylene as solvent. This solution was then further diluted by 1:10 in additional xylene. Gel permeation chromatography (GPC) indicated a weight average M_w of 74,000 and number average M_n of 27,000 g/mol for this sample, giving a polydispersity index PDI = M_w/M_n of 2.8.

The PBLG used in this study was synthesized at the MPIP by Dr M. Oosterling. The M_w was found by GPC to be 78,000 g/mol and the M_n 35,000 g/mol. Chloroform was used as the solvent. Initially, DMF was used as a solvent, with the hope of comparing the data with the detailed simulation results of Helfrich and Hentschke [37], but DMF proved to be unstable in an electric field.

4.3. PHIC and PBLG results

Both PBLG and PHIC proved to be readily orientable in an electric field during solvent evaporation. All three of the different device geometries could be used to induce orientation. The induced orientation of both polymers was nominally parallel to the electric field lines, and remained stable after the solvent was removed.

Fig. 10(a) shows a bend device at low magnification showing the overall geometry of the 3 mm × 3 mm device with the 1 mm × 1 mm square central window and lateral 1 mm × 3 mm gold pads for application of the external field. Fig. 10(b) shows a higher magnification view of the window showing the polymer drawn to region between the gold electrodes. This is the phenomenon of 'electrocapillarity', in which a solution is drawn into a region of high field in order to lower the energy of the system [38]. Electrocapillarity effects have been used to make optically active modulators [39].

Fig. 11 shows PHIC on a bend device in both unpolarized (top) and polarized light (bottom). There is a clear evidence for increased birefringence in the region nearest the origin of the radius of curvature. This observation indicates that the electric field gradient is important in determining the structural evolution, as has also been seen, for example, by Kim in liquid crystal/polymer mixtures [40]. Fig. 12 shows PHIC on a splay device, again in both unpolarized (top) and polarized light (bottom). It is now clearly evident that the intensity of transmitted light increases with increasing electric field. This is due to the fact that both the orientation and the thickness of the sample are increasing. Fig. 13 shows PHIC on a strength device, where again the increase in transmission in crossed-polars is evident as the strength of the field increases.

The transmission in crossed-polars is due to the change in both birefringence (due to increased orientation) and the sample thickness. Information about sample thickness can be obtained from interferrometric techniques using reflected light. The devices also make it possible to obtain electron microscope images from precisely the same area as observed optically. Fig. 14 shows an optical microscope image (left) and a transmission electron microscope image (right) for PHIC oriented on a bend device. From these images, it was possible to determine the relationship between image contrast in OM and TEM for samples with known amounts of thickness and degrees of orientation. It is worth noting that there are small variations in thickness within a given gap which reveal local segmentation of the curved lines used in the microfabricated device.

Fig. 15 shows an electron diffraction pattern of PHIC obtained from a region with a high degree of orientation. The schematic shows the various peaks observed, which

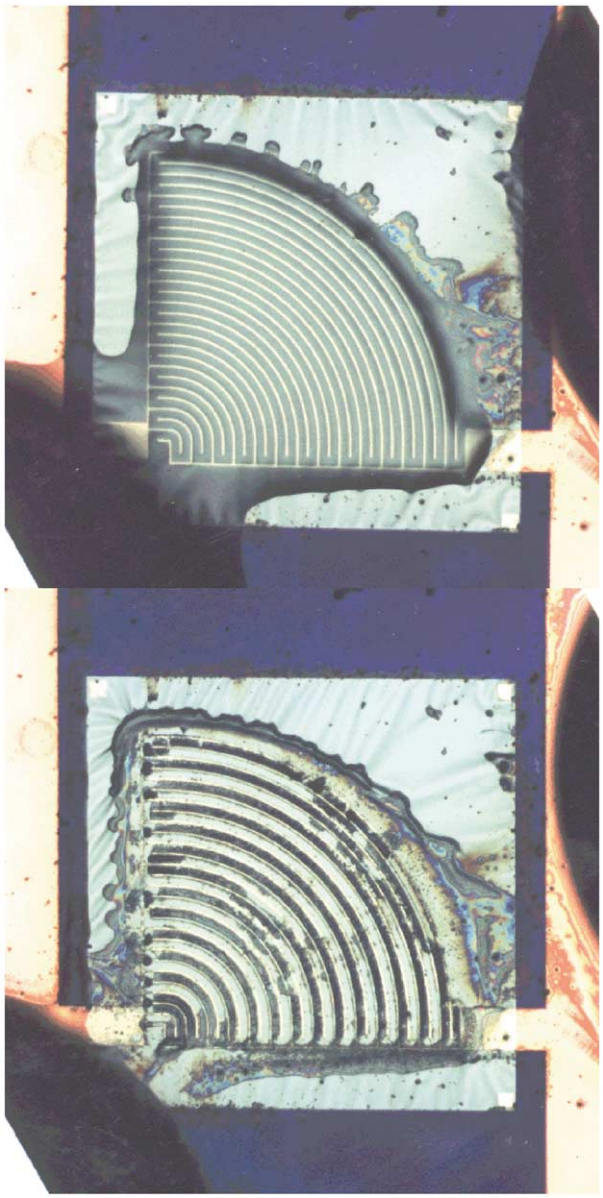

Fig. 9. Reflected light optical micrograph before (top) and after (bottom) the last phase of drying of the solvent which causes solidification of the polymer. The central square is 1 mm × 1 mm and the lines are 20 μm apart.

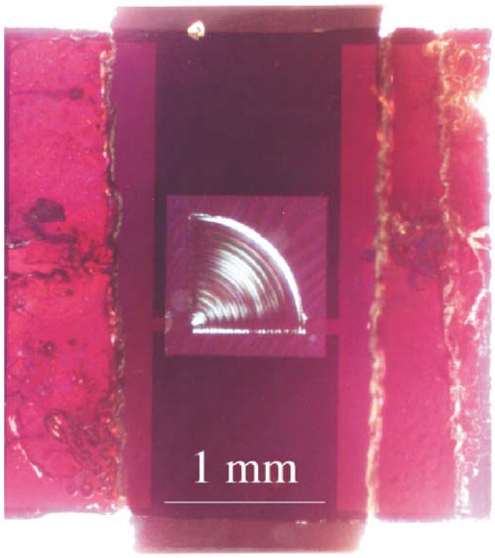

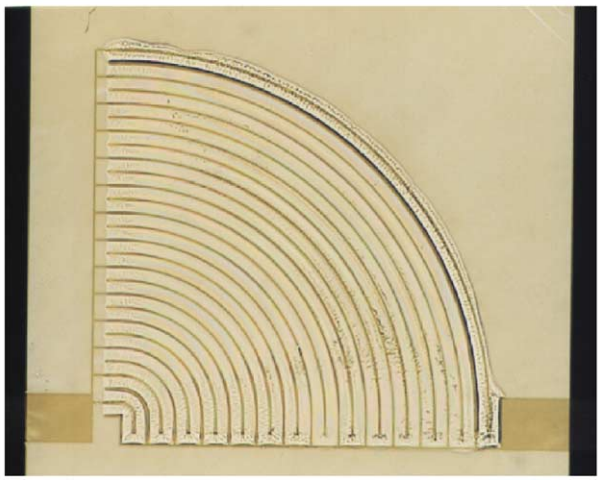

Fig. 10. Low magnification optical micrograph showing PHIC oriented on a bend device. Higher magnification view showing the polymer between the electrodes. The electrode spacing is 20 μm and the central field of the device is 1 mm × 1 mm.

were found to be generally consistent with the indexing scheme of Chen et al. [41]. Reproducible variations in the intensity of the SAED Bragg reflections were observed when tilting about an axis parallel to the molecular orientation. At zero angle, the set of three reflections nearest the equator, which roughly correspond to the (020), (031), and (03-1) indices described by Chen et al. [41], were the strongest. At higher angles (~30°), the off-axis reflection corresponding to approximately (023) was observed. Finally, at ~40° of tilt, reflections were observed at what appeared to be the (015) positions. These results reveal that the PHIC crystals were three-dimensionally ordered, and had established a preferred plane of contact with the silicon nitride substrate. It is worth remarking that this data confirms that the PHIC had been rapidly organized into

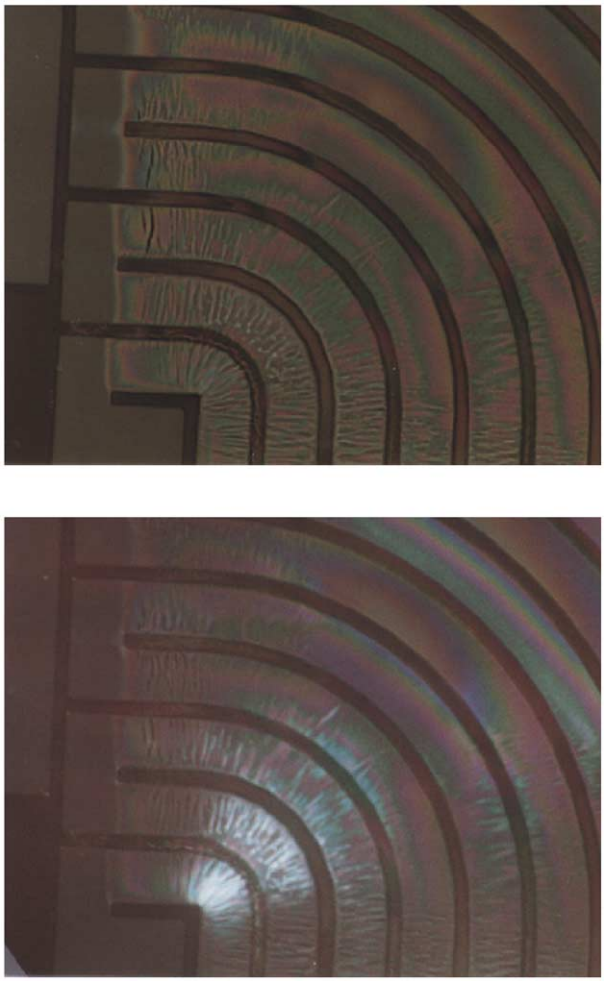

Fig. 11. Higher magnification optical micrograph of PHIC on a bend device in transmitted light (top). The bottom micrograph was taken with the polarizers nearly crossed, and indicates the higher degree of birefringence near the origin of the curvature. The electrode spacing is 20 μm.

what was essentially a single crystal texture by the process of thin film evaporation in the presence of an electric field. It was also observed that the strong equatorial reflections were the most intense and sharp at zero angle, and moved outward in scattering angle and broadened somewhat during rotation about the orientation axis. This behavior was consistent with that of a thin film of polymer molecules in good lateral registry, and suggests that the proposed pseudo-hexagonal symmetry of the unit cell may not be sufficient to describe these details of the crystalline ordering in PHIC.

Fig. 16 shows a low magnification TEM view of a bend device coated with PBLG. Higher magnification images and diffraction patterns also confirmed that the PBLG was oriented by the field. When the samples of PBLG were imaged spanning an incidental crack in the substrate they showed a fibrillar texture consistent with the development of mechanical anisotropy due to orientation.

Fig. 17 is an energy-filtered selected area electron diffraction pattern confirming that the PBLG is also oriented parallel to the field, and that this orientation is nominally

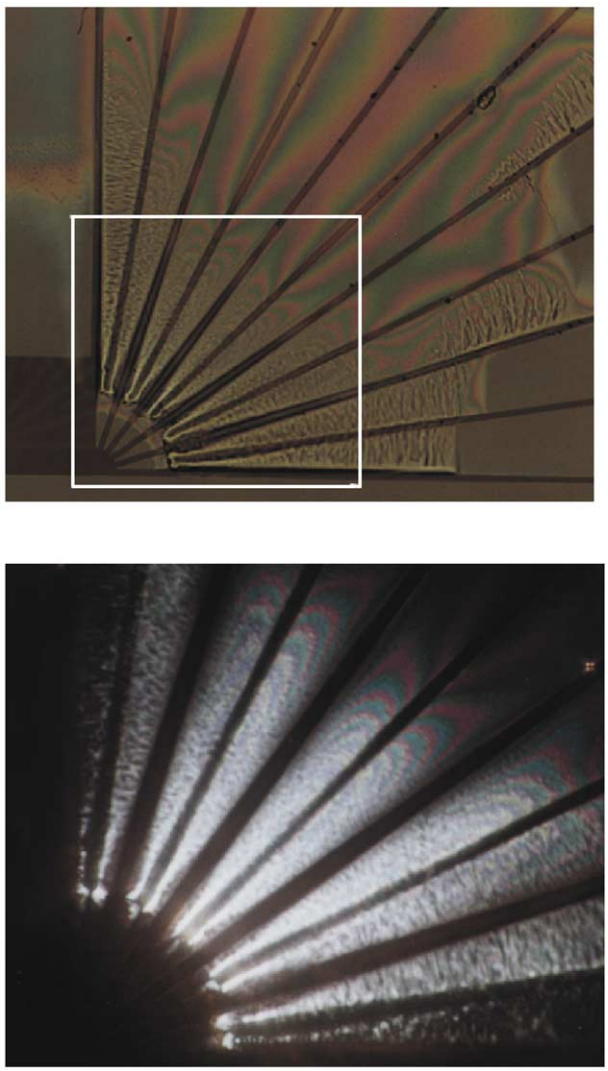

Fig. 12. Transmitted light optical micrograph of PHIC on a splay device at moderate magnification in unpolarized light (top) and at higher magnification in crossed-polars (bottom).

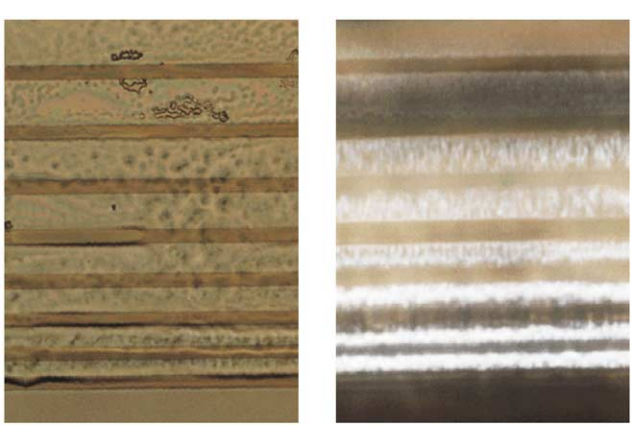

Fig. 13. Transmitted light optical micrograph of PHIC on a strength device in unpolarized light (top) and in crossed-polarizers (bottom). The minimum gap spacing in this device is 6 μm, increasing in increments of 2 μm.

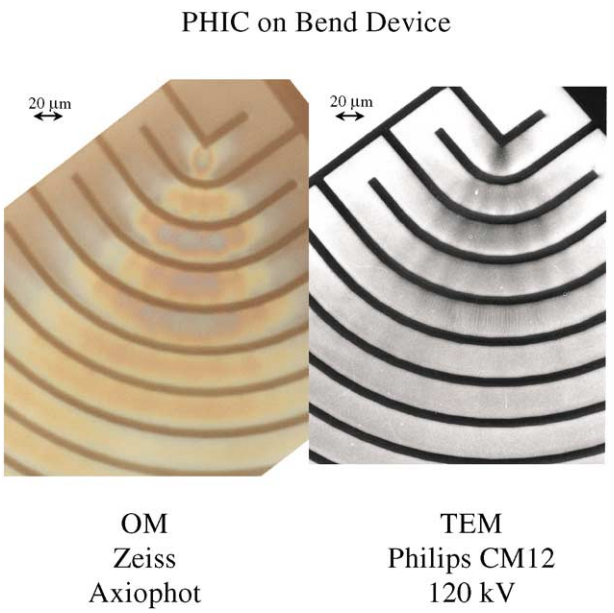

Fig. 14. Optical micrograph (left) and bright field transmission electron micrograph (right) of PHIC on a bend device. These images were taken from the same region of the same sample.

parallel to the electric field lines. The diffraction patterns showed the strong (100) and (010) equatorial reflections and fifth order layer line which were found to be generally consistent with the pseudo-hexagonal crystal form C for PBLG. Also shown in the figure is the defocused central spot in which the edge of the gold electrode can be seen, confirming the orientation of the chains in the direction of the field.

Tilting studies confirmed that the PBLG samples were also single crystal textured, with a (100) type crystal face the preferred plane of contact with the silicon nitride substrate. No evidence for a 'biaxial' orientation of the PBLG in an electric field, as described by Block and Shaw [35] was obtained in our experiments. The extent of orientation of the PBLG was higher as the field increased, as is shown quantitatively in Fig. 18. Here, the azimuthal spread of the

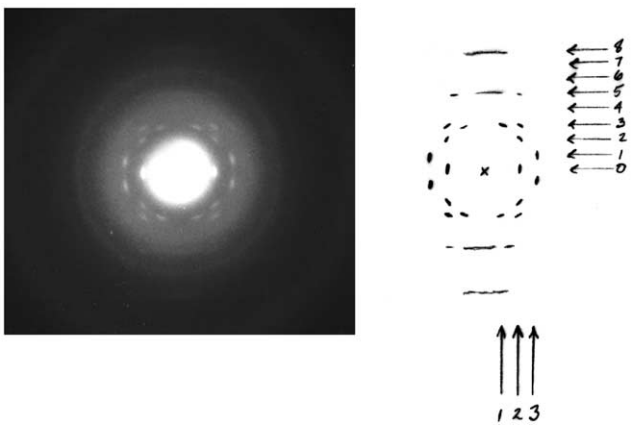

Fig. 15. Selected area electron diffraction pattern and schematic drawing of PHIC oriented in an electric field. The indexing of the pattern is consistent with the model of Chen et al. [20,41].

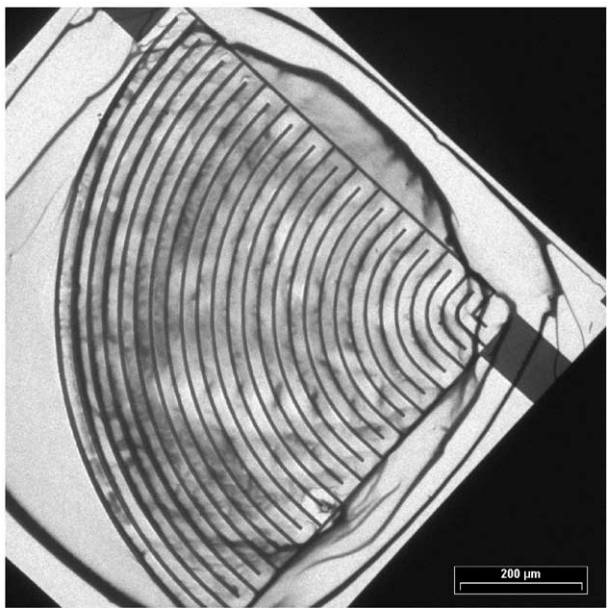

Fig. 16. Low magnification TEM image of PBLG on a bend device.

strong equatorial SAED Bragg reflection is plotted as a function of field strength. This data was obtained from a strength device with the electric field uniform in each gap. As shown in the figure, the alignment data are fit reasonably well ($R = 0.93$) to the empirical expression $\theta = 23E^{-1.1}$, with θ in degrees and E the electric field in V/μm.

Information about the specific mechanisms of electric field alignment of the liquid crystalline texture can be discerned by examining the region of a bend device nearest the origin of curvature. It is here that the electric field

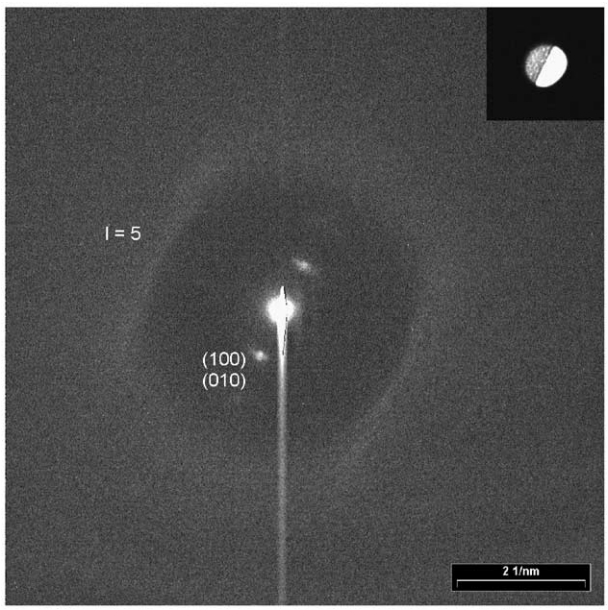

Fig. 17. Elastically filtered electron diffraction pattern of PBLG showing the orientation of the molecules is parallel to the field, as was seen for PHIC. The inset shows the defocused central spot, confirming that the molecules are normal to the electrodes.

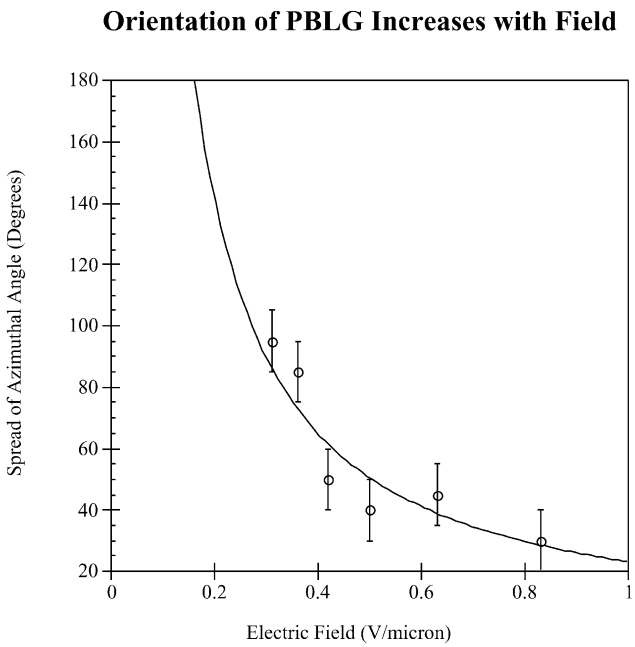

Fig. 18. Influence of electric field strength on the orientation of PBLG as observed by electron diffraction in a strength device. The plot shows the azimuthal spread of the equatorial reflection as a function of the magnitude of the field. The line corresponds to equation $\theta = 23E^{-1.1,}$ with E in V/μm and θ in degrees ($R = 0.93$).

exhibits a high degree of divergence, and is therefore expected to induce a high degree of splay into the polymer microstructure. Because of the high molecular weight, the splay constant is generally the most energetically costly in LCPs because of the need to accommodate the deformation by the aggregation of chain ends or hair pins [42,43]. It was therefore not at all clear what an LCP would do in response to the locally divergent electric field produced in a bend device.

Fig. 19 shows an example of what can happen under these circumstances for PBLG. This bright field image shows texturing due to cracking of the PBLG film, which serves to locally decorate the orientation. The extent of this cracking was found to be a function of the rate of solvent evaporation. The molecules are nominally oriented in a manner which is similar to that of the cracks, although it has not yet been established that the cracks are precisely the same as the local orientation. In polyparaphenylene terephthalamide, for example, it has been found that crystals with a rhombohedral shape can be formed in which the surfaces are at a significant axis to the molecular direction [44], and this possibility cannot be completely excluded until higher resolution images of the PBLG lattice can be obtained. Nevertheless, this cracking made it possible to monitor the nature and extent of the organization of the PBLG as function of position in the gap.

It is clear from Fig. 19 that the extent of orientation of the PBLG texture was largest near the corner of the device, and decreases as toward the opposite wall. Individual orientational defects (disclinations) could be identified, and these

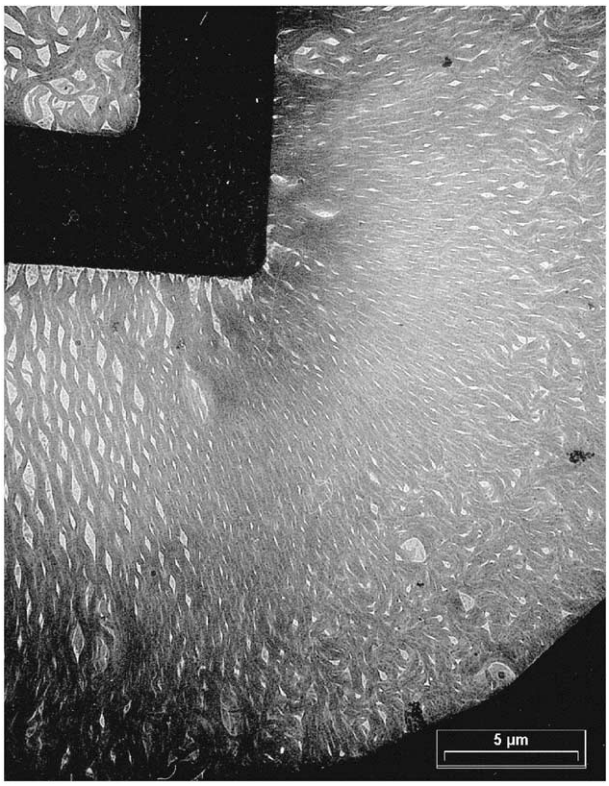

Fig. 19. High magnification bright field image of the region of a bend device near the origin of the curvature, where the molecules are subjected to severe splay deformations. The film shows a cracked texture which is evidently generated during solvent evaporation. There is evidence for specific +1/2 and −1/2 defects in the structure, but these defects are only present on the side of the gap away from the origin of curvature. The potential used in this experiment was 30 V.

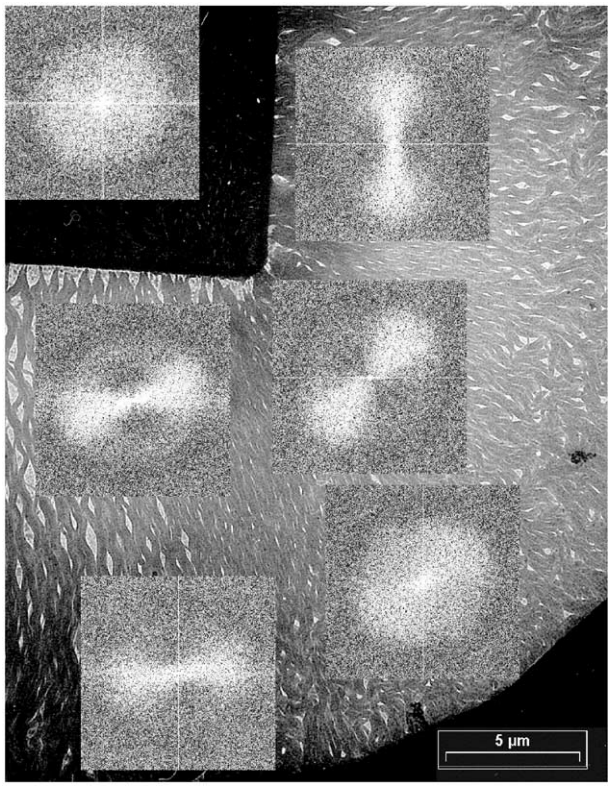

Fig. 20. Digital FFTs inset on top of Fig. 19 in the corresponding locations showing the decrease in orientation of the texture from the inside of the gap to the outside. Also shown is the fact that there is no net orientation in the upper right-hand corner where there is no electric field.

were clearly clustered together near this wall. Both +1/2 and −1/2 defects were observed, as well as some occasional +1 and −1 singularities. That the extent of order varied across the gap is confirmed by Fig. 20, in which digital FFTs of the image are superposed on top of the respective areas from which they were taken. There was clearly an orientation parallel to the field lines, and the extent of this orientation decreased across the field. Also shown is that the PBLG molecules located where there was little or no field (upper left) remained essentially unoriented.

The presence of disclination defects on the side of the gap with the larger radius of curvature was seen to be a consistent observation under these experimental conditions. As the average radius of curvature increased, the width of this defective zone decreased, until at a sufficiently high radius of curvature no more disclination defects were observed (Fig. 21).

These observations indicate that both the magnitude and nature of the electric field influences the structural organization that is induced. The fact that the defect density is a function of the field geometry has implications for the fiber spinning process, in which it is well established that fairly intense shear fields are necessary to obtain optimum orientation, and therefore tensile properties, of fibers

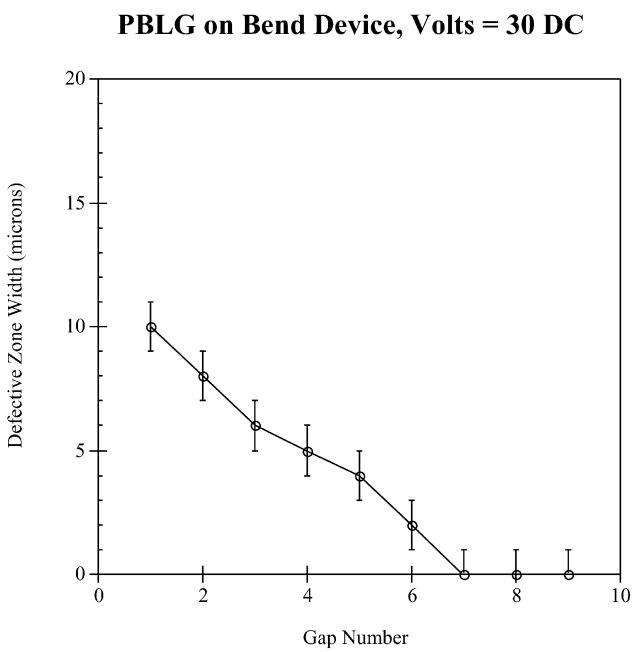

Fig. 21. Width of the defective zone in a bend device for PBLG with an external voltage of $V = 30$ V DC. The smallest gap numbers are those closest to the origin of curvature. As the radius of curvature increases, the size of the defective zone decreases until it can no longer be discerned beyond gap number 7.

produced from liquid crystalline solutions. If the field is not sufficiently high to eliminate rotational defects from the microstructure, this is likely to lead to substantially decreased mechanical properties.

It is also worth considering the stability of disclination defects in an oriented liquid crystalline material. For a paranematic material, there is a difference in energy between the up $(+n)$ and down $(-n)$ orientations of the molecule. This means that for half-strength defects, there will necessary be a region at which there is an incompatibility in orientation, leading to a domain wall of higher energy (Fig. 22).

Another defect which may be important in oriented LCPs is the clinicity switching from 'up' to 'down' as described earlier and as shown schematically in Fig. 23. In this figure, molecular models of poly(methyl isocyanate) are shown with 'left' and 'right' helix reversals, with an up chain meeting a down chain, and with a down chain meeting an up chain. For poly(alkyl isocyanates), these variations in clinicity can be achieved independently of the handedness of the chain. The ability to switch from up to down will depend on chain microstructure, and is not possible in chiral poly(peptides) such as PBLG, for example. The geometry and energetics of these up–down defects in clinicity have been discussed by Carbeck and Rutledge for poly(vinylidene fluoride) [45]. It should be made clear that our data obtained to date neither confirms nor precludes the presence of these hypothesized defects in chain clinicity.

The role of clinicity defects is also expected to be important in stabilizing the energetics of defects in chain trajectory, which have been called 'hairpins' for a general nematic chain [46] and 'rollers' in dipoled chains [47]. By introducing defects in the chain

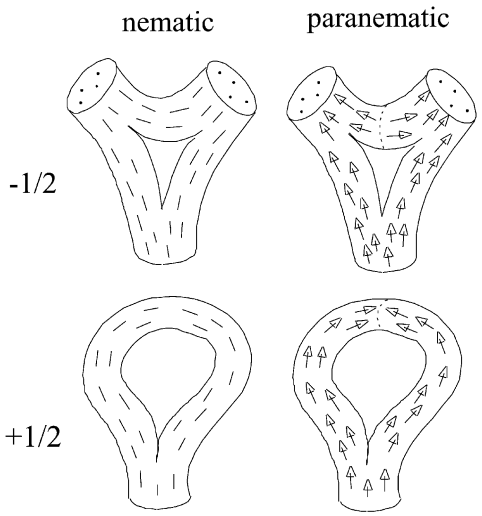

Fig. 22. Schematic diagrams of $+1/2$ and $-1/2$ strength disclinations in paranematics. As shown in the diagram, such half-strength defects require interactions between dipoles of opposite sense at some position around the core. They therefore would be expected to be unstable in a sufficiently strong external field.

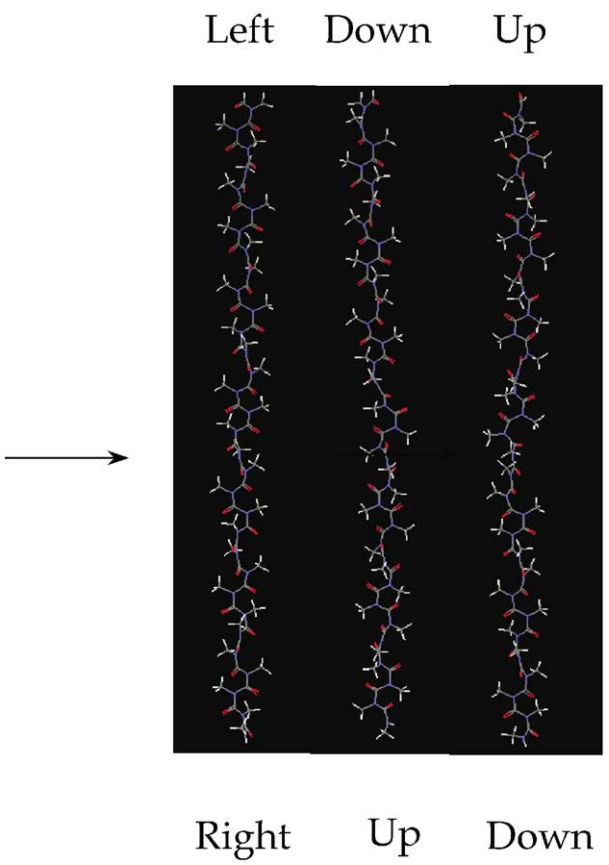

Fig. 23. Molecular models of defects in helical poly(alkyl isocyanate) chains with dipoles. Both defects in handedness (left–right) as well as clinicity (up–down) are expected. Such defects in clinicity are not likely in the PBLG chains, which are polypeptides with a fixed chirality.

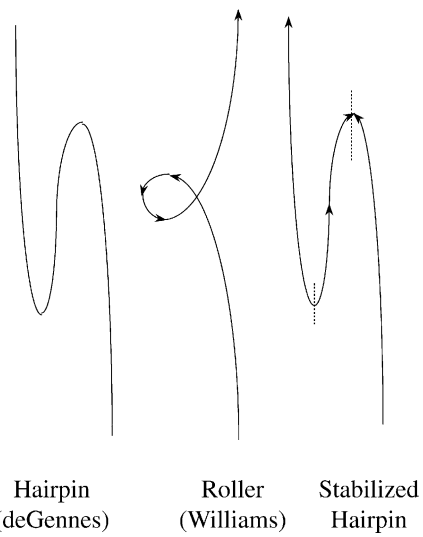

Fig. 24. Molecular models of hairpin defects in a nematic chain (deGennes, 1992) and a 'roller' in a dipoled chain [47]. If a chain with a hairpin or roller defect also had a clinicity defect (Fig. 23), it would be stabilized in the field and would therefore become very difficult to remove.

clinicity, it would be possible to stabilize the free energy of a roller. This would trap the chain reversals in place, and would make such a defect much more difficult to eliminate (Fig. 24).

4.4. Other materials

A number of non-polar polymers were also investigated to see if there might be any influence of the electric field on the organization of these materials during solvent evaporation. These included polyethylene (PE), the carbazolyl-substituted diacetylene DCHD, and two new bithiazole-containing polymers prepared by Prof. M. David Curtis's group at the University of Michigan. While it was recognized that any observed effect would be smaller than in the polymers with inherent dipoles, non-polar polymers have been processed into oriented structures by electric fields, such as in electrospinning. Also, it was thought that it might be possible for anisotropic shapes to respond due to variations in dielectric constant, as in the case of block copolymers. However, no experimentally significant orientation with respect to the field was observed for any of these less-polar materials in fields as high as 1.5 V/μm.

Electric fields were also used to orient a number of other materials including block copolymers in which one of the components could be converted to a ceramic material, polyphthalocyanines, and a rod-coil diblock copolymer of isoprene-*b*-hexyl isocyanate [26]. The composition was chosen such that it would lie in the arrowhead regime [41]. The M_w of this sample was evaluated by GPC as 11,400 PI-*co*-1,580,000 PHIC. The microphase-separated structure of this relatively high M_w rod-coil which developed was not as well defined as that seen previously [41]. The sample formed a stable gel in a 1% solution. The polymer developed a dramatic optical texture which responded to the field. TEM showed that it particularly avoided filling the corners, where there would have been large amounts of splay deformation. This is consistent with the expectation that sample prefers to have a layered smectic-like structure, which does not accommodate splay. It was confirmed by SAED that a high degree of orientation of the PHIC molecules parallel to the field was achieved.

Experiments were also performed on a small molecule liquid crystal (4′-pentyl-4-biphenyl carbonitrile) that exhibits a nematic mesophase at room temperature. This molecule responded rapidly to the field, showing birefringence due to the induced orientation. For devices with a 20 μm gap, the sample went isotropic for applied fields above 133 V. At low fields, the sample was found to 'shimmer' in the optical microscope, and showed evidence for single disclination lines. With increasing field, it was observed that these lines would become locally straight, and deformation would localize into well-defined kinks, resulting in a zig-zag conformation of the defect. The disclination lines would occasionally be seen to stabilize between the electrodes (this was specifically observed at 12 V), and the kinks were observed to wander along the length of the line defect. The time scale of the oscillations in disclination motion decreased with increasing voltage, but these rates were not quantified. These observations were very reproducible and reversible.

5. Discussion

Our results suggest that the kinetics of solvent loss is a critical component of the structure which develops in this process. Wang and co-workers have examined molecular motions in lyotropic LCP mesophases (P-4-BCMU) during slow solvent annealing [27,48,49]. Evidence was obtained for chain end segregation, and variations in the lamellar thickness near disclination cores were interpreted in terms of the lateral and longitudinal motion of the molecules. More work is necessary to explore similar phenomena in these systems where there is also an external electric field.

We have observed that the geometry of the field influences the defect density after solidification. This corresponds with the well-known fact that higher strain fields can lead to fibers with better tensile properties, presumably due to a lower disclination defect density in the filament. It was also found that the reorganization near a disclination core due to crystallization was similar to that seen in an external field, leading to an estimate of a characteristic 'crystallization length'.

5.1. Possibilities for future studies

The polymers used in this study were not fractionated, and did not have widely different molecular weights. Bur and Fetters have emphasized the need to use monodisperse samples to isolate effects of the transition from small, rigid chains to long, flexible systems, particularly for these 'worm-like' molecules. Future work will need to focus on systems with more well-controlled polydispersities. Potentially available synthetic routes include the organotitanium(IV)-based living polymerization described by Patten and Novak [50] for poly(alkyl isocyanates), and the use of genetic engineering to create monodisperse samples of PBLG [51]. The importance of chain end aggregation was shown by the formation of stable layered phases with smectic order in these latter materials.

Additional studies need to be conducted with variations in evaporation rate, and to explore the influence of field geometry in more detail. Of particular interest will be methods to better control the evaporation rate, such as by using an environmental chamber during sample preparation. Alternatively, one could consider the use of alternative, non-polar solvents to change the volatility. These studies will need to recognize the potential for forming crystal-solvate phases during solvent loss.

It was found that AC fields could also be used to induce alignment. It is expected that the materials should not

exhibit polar order after solidification in this case. This possibility is being actively explored by Dr Mathias Flörsheimer, who has constructed a microscope to examine the second-order non-linear optical properties of polymer thin films [52]. Our devices should be ideal for testing the performance of this new instrument. The ability to distinguish between DC (net dipole orienting) and AC (no net dipole orienting) response should be of particular interest. With AC fields it will also be able to investigate the role of frequency on the alignment process.

It is also possible to consider alternative device geometries, such as creating a locally divergent extensional field analogous to that created to study elongational flow fields, to look at molecular elongation in a similar manner. Finally, one could consider adding a perpendicular magnetic field to see changes that would be mobile carrier-sign dependent, as in the Hall effect.

6. Conclusions

1. Lyotropic LCP (PHIC and PBLG) thin films can be rapidly oriented in a controlled manner using both DC and AC electric fields.
2. The degree of induced orientation is a function of the strength and geometry of the electric field.
3. The microstructure of the samples can be examined by both OM and TEM. The micropatterned lines can be used to facilitate corroborative experiments from the same region of the sample using the different characterization techniques.
4. Tilting experiments confirm that the PHIC thin films have a three-dimensional texture. PBLC shows evidence for three-dimensional texturing as well, although the out-of-plane ordering does not appear to be as well developed as for PHIC.
5. Variations in thickness, as well as the perfection of orientation have been seen when the field is forced to locally diverge (splay) between curved electrodes. The defect structure changes as the geometry of the field changes.

Acknowledgments

Considerable assistance and support were provided throughout the course of this work by Dr Alexander DuChesne and Prof. Gerhard Wegner, and their help is gratefully acknowledged. The author would also like to thank Dr Gunter Lieser and Gunner Glasser for technical assistance, Dr M. Oosterling for synthesis of the PBLG, Dr Gary Bordonario at the Cornell National Nanofabrication Facility, Dr Libby Louie for assistance in device fabrication at the NNF, and Prof. Thomas Russell of the University of Massachusetts at Amherst his inspiration and encouraging discussions. Funding for this research was provided by the Alexander von Humboldt Stiftung (fellowship to DCM), the Max-Planck Institut für Polymerforschung in Mainz, and the National Science Foundation.

References

[1] Muthukumar M, Ober CK, Thomas EL. Competing interactions and levels of ordering in self-organizing polymeric materials. Science 1997;277:1225–32.
[2] Havelka KO, Filisko FE. Progress in electrorheology: science and technology of electrorheological materials. New York: Plenum Press; 1995.
[3] Jaworek T, Neher D, Wegner G, Wieringa RH, Schouten AJ. Electromechanical properties of an ultrathin layer of directionally aligned helical polypeptides. Science 1998;279:57–60.
[4] Sessler GM. Electrets, 2nd enlarged ed.; 1987.
[5] Hudson SD, Thomas EL. Disclination interaction in an applied field: stabilization of the Lehman cluster. Phys Rev A 1991;44(12):8128.
[6] Körner H, Shiota A, Bunning TJ, Ober CK. Science 1996;272(5259): 252.
[7] Shiota A, Ober CK. Orientation of liquid crystalline epoxides under AC electric fields. Macromolecules 1997;30:4278–87.
[8] Morkved TL, Lu M, Urbas AM, Ehrichs EE, Jaeger HM, Mansky P, Russell T. Local control of microdomain orientation in diblock copolymer thin films using electric fields. Science 1996;273:931.
[9] Morkved TL, Lopes WA, Hahm J, Sibener SJ, Jaeger HM. Silicon nitride membrane substrates for the investigation of local structure in polymer thin films. Polymer 1998;39(16):3871–5.
[10] Amundson K, Helfand E, Quan X, Smith S. Alignment of lamellar block copolymer microstructure in an electric field. 1. Alignment kinetics. Macromolecules 1993;26:2698–703.
[11] Frank FC. Discuss Faraday Soc 1958;25:10.
[12] Chaikin P, Lubensky T. Principles of condensed matter physics, 1st ed. Cambridge: Cambridge University Press; 1995.
[13] Bur A, Fetters LJ. Chem Rev 1976;76:727.
[14] Aharoni SM. *n*-Nylons: their synthesis, structure, and properties. Chichester, England: Wiley; 1997.
[15] Shmueli U, Traub W, Rosenbeck K. Structure of poly(*N*-butyl isocyanate). J Polym Sci 1969;A-2(7):515–24.
[16] Troxell TC, Scheraga HA. Electric dichroism and polymer conformation. 2. Theory of electric dichroism, and measurements on poly(butyl isocyanate). Macromolecules 1971;4(5):528–37.
[17] Troxell TC, Scheraga HA. Electric dichroism and polymer conformation. 1. Theory of optical properties of anisotropic media, and method of measurement. Macromolecules 1971;4(5):519–27.
[18] Tsevtkov VN, Ryumtsev YI, Shtennikova IN. Polym Sci USSR 1971; 13:579.
[19] Bur AJ, Roberts DE. Rodlike and random-coil behavior of poly(*N*-butyl isocyanate) in dilute solution. J Chem Phys 1969;51(1):406–20.
[20] Chen JT, et al. Zigzag morphology of a poly(styrene-*b*-hexyl isocyanate) rod-coil block-copolymer. Macromolecules 1995;28(5): 1688–97.
[21] Green MM, et al. A helical polymer with a cooperative response to chiral information. Science 1995;268:1860.
[22] Onsager L. The effects of shape on the interaction of colloidal particles. Ann NY Acad Sci 1949;51(4):627–59.
[23] Flory PJ. Phase equilibria in solutions of rod-like particles. Proc R Soc Lond, Ser A 1956;234(1196):73–89.
[24] Khoklov AR, Semenov AN. Influence of external fields on the liquid-crystalline ordering in solutions of stiff-chain macromolecules. Macromolecules 1982;15:1272–7.
[25] Filisko FE, Henley S, Quist G. Recent developments in the properties and composition of electrorheological fluids. J Intell Mater Syst Struct 1999;10(6):476–80.
[26] Aronson CL. Structure–property relationships for *n*-alkyl isocyanate

containing polymers. Macromolecular science and engineering. Ann Arbor: The University of Michigan; 1999. p. 263.
[27] Wang W, Hashimoto T, Lieser G, Wegner G. Elastic constant anisotropy, core structure of wedge disclinations and optical texture of main-chain P-4-BCMU liquid crystals. J Polym Sci, B: Polym Phys Ed 1994;32:2171–86.
[28] Hudson SD, et al. Disclination core structure in rigid and semiflexible main-chain polymer nematic liquid crystals. Macromolecules 1993; 26:1270–6.
[29] Takashima S. Electrical properties of biopolymers and membranes. Bristol: IOP Publishing Ltd; 1989.
[30] Cohen Y, Thomas EL. Microfibrillar network of a rigid rod polymer. 2. Small angle X-ray scattering. Macromolecules 1988;21:436.
[31] Cohen Y, Thomas EL. Microfibrillar network of a rigid rod polymer. 1. Visualization by electron microscopy. Macromolecules 1988;21: 433.
[32] Cohen Y, Dagan A. Phase transformations in concentrated solutions of poly(gamma-benzyl L-glutamate). Macromolecules 1995;28: 7638–44.
[33] Sasaki S, Hikata M, Shiraki C, Uematsu I. Molecular aggregation and gelation in poly(gamma-benzyl L-glutamate) solutions. Polym J 1982; 14(3):205–13.
[34] Sasaki S, Tokuma K, Uematsu I. Phase-behavior of poly(gamma-benzyl L-glutamate) solutions in benzyl alcohol. Polym Bull 1983; 10(11-1):539–46.
[35] Block H, Shaw CP. Second-harmonic generation in poly(alpha-amino acid) and polyisocyanate films. Polymer 1992;33(11):2459–62.
[36] DuChesne A. Energy filtering transmission electron microscopy of polymers—benefit and limitations of the method. Macromol Chem Phys 1999;200(8):1813–30.
[37] Helfrich J, Hentschke R. Molecular dynamics simulation of macromolecular interactions in solution—poly(gamma-benzyl glutamate) in dimethylformamide and tetrahydrofuran. Macromolecules 1995;28:3831.
[38] Adamson A. Physical chemistry of surfaces, 6th ed. New York: Wiley; 1997.
[39] Lea MC. Optical modulators based on electrocapillarity. Opt Lett 1981;6(8):395–7.
[40] Kim Y, Francl J, Taheri B, West JL. A method for the formation of polymer walls in liquid crystal/polymer mixture. Appl Phys Lett 1998; 72:2253..
[41] Chen JT, et al. Zigzag morphology of a poly(styrene-*b*-hexyl isocyanate) rod-coil block copolymer. Macromolecules 1995;28: 1688–97.
[42] Mazelet G, Kleman M. Observation of defects in a polyester nematic phase. Polymer 1986;27:714–20.
[43] Hobdell J, Windle A. A numerical technique for predicting microstructure in liquid crystalline polymers. Liq Cryst 1997;23(2): 157–73.
[44] Roche EJ, Allen SR, Gabara V, Cox B. Thin-film morphology and crystal-structure of the poly(p. phenylene terephthalamide) sulfuric-acid system. Polymer 1989;30(10):1776–84.
[45] Carbeck JD, Rutledge GC. A method for studying conformational relaxations by molecular simulation: conformational defects in alpha-phase poly(vinylidene fluoride). Macromolecules 1996;29(15): 5190–9.
[46] deGennes PG. In: Ciferri A, Krigbaum WR, Meyer R, editors. Polymer liquid crystals. New York: Academic Press; 1982.
[47] Williams DRM. Rollers—a new type of defect in dipoled polymer chains. J Phys A: Math Gen 1991;24:4427–44.
[48] Wang W, Lieser G, Wegner G. Bright field image of banded texture in lyotropic liquid crystals of a polydiacetylene. Makromol Chem 1993; 194:1289–97.
[49] Wang W, Lieser G, Wegner G. Extended-chain lamellar structure and chain segregation in lyotropic liquid crystals of poly{5,7-dodecadyne-1,12-diol bis[((4-butoxycarbonyl)methyl)urethane]}. Macromolecules 1994;27:1027–32.
[50] Patten TE, Novak BM. J Am Chem Soc 1991;113:5065.
[51] Yu SM, et al. Smectic ordering in solution and films of a rod-like polymer owing to monodispersity of chain length. Nature 1997; 389(6647):167–70.
[52] Flörsheimer M, et al. Second-harmonic microscopy—a quantitative probe for molecular surface order. Adv Mater 1997;9(13):1061.